Available online at www.sciencedirect.com
SCIENCE DIRECT®
Journal of Solid State Chemistry 178 (2005) 3027–3039
JOURNAL OF SOLID STATE CHEMISTRY
www.elsevier.com/locate/jssc

Chemical diffusion of oxygen in tin dioxide: Effects of dopants and oxygen partial pressure

B. Kamp, R. Merkle*, R. Lauck, J. Maier

Max-Planck-Institut für Festkörperforschung, Heisenbergstraße 1, 70569 Stuttgart, Germany

Received 12 May 2005; received in revised form 12 July 2005; accepted 19 July 2005
Available online 22 August 2005

Abstract

Tin dioxide $SnO_{2-\delta}$ is a pronounced n-type electron conductor due to its oxygen deficiency. This study investigates the rate of chemical diffusion of oxygen in $SnO_{2-\delta}$ single crystals, which is a crucial step in the overall stoichiometry change of the material. The chemical diffusion coefficient D^{δ} was determined from conductivity- and EPR-relaxation methods. The temperature dependence was found to be $D^{\delta} = \exp(-4 \pm 2)\,cm^2\,s^{-1}\,\exp(-(1.1 \pm 0.3)\,eV/kT)$. The dependence on crystal orientation, dopant content and oxygen partial pressure was below experimental error. The latter observation leads to the conclusion that the chemical diffusion coefficient is close to the diffusion coefficient of oxygen vacancies. Along with the relaxation process resulting from the chemical diffusion of oxygen, additional processes were observed. One of these was attributed to complications in the defect chemistry of the material. The relevance of the results for the kinetics of drift processes of Taguchi sensors is discussed.

Keywords: Oxygen diffusion; EPR; Trapping reaction; SnO_2; Drift processes; Taguchi sensor; Defect chemistry

1. Introduction

1.1. Stoichiometry changes in $SnO_{2-\delta}$ and drift of Taguchi sensors

Tin dioxide $SnO_{2-\delta}$ is an n-type semiconductor which is applied for resistive gas sensors of the Taguchi type or for optically transparent conductive layers. Taguchi sensors can detect redox-active gases such as NO_x or CO. They are typically composed of porous semiconducting ceramics, mostly $SnO_{2-\delta}$. The sensing principle is based on the variation of the surface space charge layer (electronic depletion layer). The latter depends on concentration and nature of the adsorbed gases, which leads to changes in the overall resistivity of the ceramics. Two effects related to oxygen transport in the material can occur which will cause a drift of Taguchi sensors:

(i) Changes of oxygen stoichiometry comprise surface exchange reaction and chemical diffusion of oxygen. The changes in oxygen defect concentration affect both bulk and space charge regions. Several authors [1,27] have identified this process as a cause for drift of Taguchi sensors.
(ii) The second effect that we refer to as "field-induced migration" does not necessitate an exchange of oxygen with the surrounding gas phase. Changes in the space charge potential upon gas adsorption will cause the charged oxygen vacancies to redistribute in the space charge region and thus affect the conductivity.

It should be noted that this division in two separate effects is somewhat simplistic. After a change in $p(O_2)$, both processes occur. If the width of the space charge

*Corresponding author. Fax: +49 711 689 1722.
E-mail address: s.weiglein@fkf.mpg.de (R. Merkle).

0022-4596/$ - see front matter © 2005 Elsevier Inc. All rights reserved.
doi:10.1016/j.jssc.2005.07.019

layer is comparable to the grain size, the two effects cannot be separated at all. A more detailed discussion and numerical simulations of the respective kinetics has been presented in a previous paper [2].

The understanding of the drift of Taguchi sensors necessitates comprehensive measurements of the chemical diffusion coefficient of oxygen (D^{δ}). Though several authors have reported measurements of this quantity [3–6] a systematic study taking into account the impact of dopant content and oxygen partial pressure has not been performed to our knowledge. In $SnO_{2-\delta}$ chemical diffusion of oxygen is the simultaneous transport of oxygen vacancies $V_O^{\bullet\bullet}$ and electrons e′. Together with the surface exchange reaction describing the transfer of oxygen from the gas phase into the solid it constitutes the oxygen incorporation process leading to the overall stoichiometry change.

In the present study, chemical diffusion of oxygen was investigated by means of relaxation experiments on single crystals of SnO_2 (thus avoiding complications resulting from grain boundaries) as a function of $p(O_2)$ and dopant content. Changes in oxygen defect concentration after sudden changes in oxygen partial pressure were followed by conductivity and EPR measurements of redox-active transition metals that are present as impurities or have been deliberately introduced. These ions change their valence according to the local changes in the oxygen stoichiometry [7]. Since tin dioxide crystallizes in the tetragonal rutile structure, diffusion coefficients along the *a*- and *c*-axis have to be distinguished.

1.2. Bulk defect chemistry in SnO_2

$SnO_{2-\delta}$ is an n-type electronic conductor in which the oxygen deficiency δ is caused by oxygen vacancies ($V_O^{\bullet\bullet}$). In pure $SnO_{2-\delta}$, the latter defects are charge-compensated by conduction electrons (e′) [3,5,8]. From data in [8,9] it can be calculated that the deviation δ reaches a maximum value of 0.03 at 900 °C, before the material is reduced to Sn_3O_4. In the following we give a brief overview of the basic defect-chemical relations, for a more detailed description see Ref. [3]. The oxygen exchange equilibrium can be described by (using the Kröger–Vink notation):

$$O_O^x \rightleftharpoons V_O^{\bullet\bullet} + 2e' + \tfrac{1}{2}O_2, \tag{1a}$$

$$K_O = [V_O^{\bullet\bullet}][e']^2 p(O_2)^{1/2}, \tag{1b}$$

where $p(O_2)$ is the oxygen partial pressure, K_O is the respective mass action constant and square brackets indicate concentrations. The presence of Schottky defects has been proposed for temperatures above 700 °C [10]:

$$SnO_{2,bulk} \rightleftharpoons SnO_{2,surf} + 2V_O^{\bullet\bullet} + V_{Sn}^{''''}, \tag{2a}$$

$$K_S = [V_O^{\bullet\bullet}]^2[V_{Sn}^{''''}], \tag{2b}$$

where $V_{Sn}^{''''}$ are fully ionized tin vacancies. If redox-active impurities (deep donors/acceptors) are present, the change of their valence state has to be taken into account. Iron in SnO_2 will occupy tin sites in the lattice [11] and undergo a valence change from iron(III) (Fe_{Sn}') to iron(II) (Fe_{Sn}'') upon reduction:

$$Fe_{Sn}'' \rightleftharpoons Fe_{Sn}' + e', \tag{3a}$$

$$K_{Fe} = \frac{[e'][Fe_{Sn}']}{[Fe_{Sn}'']}. \tag{3b}$$

Neglecting tin vacancies, the condition of electroneutrality is given by

$$[A'] + [Fe_{Sn}'] + 2[Fe_{Sn}''] + [e'] = 2[V_O^{\bullet\bullet}] + [D^{\bullet}], \tag{4}$$

where [A′] and [D•] denote the concentrations of additional, redox-inactive (i.e. shallow) acceptors or donors, respectively. If we neglect valence changes of the dopants and the Schottky equilibrium, simple power laws for the partial pressure dependence of the electron concentration are obtained from Eqs. (1b) and (4). Assuming that the electronic mobility does not vary with $p(O_2)$ we obtain for the conductivity σ [3,5]:

$$\sigma \propto [e'] \propto p(O_2)^{-n}, \tag{5}$$

with n being

(i) pure material (intrinsic) case : $n = 1/6$,
(ii) acceptor − doped case : $n = 1/4$,
(iii) donor − doped case : $n = 0$.

For the EPR measurements, the concentration variation of the EPR-active species (e.g. Fe^{3+}) with oxygen partial pressure is decisive [7]. If we assume that iron predominantely has the oxidation state +2, i.e. $[Fe_{Sn}'] \ll [Fe_{Sn}''] \cong [Fe]_0$ ($[Fe]_0$ = total iron concentration), which will occur at sufficiently low oxygen partial pressure, then we derive the following [7] ($m = 1/6$ intrinsic case, $m = 1/4$ acceptor doped):

$$[Fe_{Sn}'] \propto p(O_2)^m. \tag{6a}$$

At sufficiently high oxygen partial pressure all Fe^{2+} is fully oxidized to Fe^{3+}, i.e.

$$[Fe_{Sn}'] = [Fe]_0 = \text{const}. \tag{6b}$$

1.3. Dependence of chemical diffusion coefficients on oxygen partial pressure and dopant content

In the following we give the basic relations that link the chemical diffusion coefficient to oxygen partial pressure and the concentration of redox-active species (for details see [12]). In the case of an n-type conductor with predominant electronic conduction such as $SnO_{2-\delta}$, the chemical diffusion coefficient of oxygen D^{δ} depends on the diffusion coeffecient $D_{V_O^{\bullet\bullet}}$ of oxygen

vacancies according to

$$D^{\delta} = D_{V_O^{\cdot\cdot}} \left(1 + \frac{4[V_O^{\cdot\cdot}]}{[e']}\chi\right). \quad (7)$$

Here χ is the "trapping factor" [12], which has a value of 1 if redox-active impurities are absent or if the conditions are such that either only the oxidized or only the reduced state occurs. If on the other hand reversible trapping occurs, the trapping factor can assume values between zero and one. In this way, depending on dopant content and oxygen partial pressure, the chemical diffusion coefficient may be lowered by orders of magnitude compared to a fixed valence situation. Here we assume that several redox-active dopants T_1, T_2, ... are present that trap electrons according to

$$T_1^{m_1'} \rightleftharpoons T_1^{(m_1-1)'} + e',$$

$$T_2^{m_2'} \rightleftharpoons T_2^{(m_2-1)'} + e' \ldots . \quad (8)$$

For the trapping factor the following relation can be obtained [13]:

$$\chi = \left(1 + \frac{K_{T_1}[T_1]_0}{\left(K_{T_1} + [e']\right)^2} + \frac{K_{T_2}[T_2]_0}{\left(K_{T_2} + [e']\right)^2} + \cdots\right)^{-1}, \quad (9)$$

where $[T_1]_0$, $[T_2]_0$ ... are the respective total dopant concentrations and K_{T_1}, K_{T_2} ... are the equilibrium constants of the reactions (8). As [e′] is unambiguously determined by dopant concentration, temperature and $p(O_2)$ according to the defect model, this also holds for χ and D^{δ}. Even though we presuppose that the oxide is predominantly electronically conducting ($\sigma_{eon} \gg \sigma_{ion}$) we must distinguish the following limiting cases.

(i) *Pure material*: The intrinsic concentration of electrons and oxygen vacancies is much higher than that of other defects. The resulting electroneutrality condition is $[e'] = 2[V_O^{\cdot\cdot}]$. Since the trapping factor is close to unity we obtain from Eq. (7):

$$D^{\delta} \approx 3D_{V_O^{\cdot\cdot}}(T). \quad (10)$$

The chemical diffusion coefficient is thus independent of $p(O_2)$ and electron concentration.

(ii) *Shallow donor-doped case*: Since in this case we can write $[e'] = [D^{\cdot}] \gg [V_O^{\cdot\cdot}]$ Eq. (7) becomes

$$D^{\delta} \approx D_{V_O^{\cdot\cdot}} \quad (11)$$

with D^{δ} again being $p(O_2)$ independent.

(iii) *Shallow acceptor-doped case*: If the material is primarily doped with redox-inactive acceptors A′, the electroneutrality condition can be written as $[A'] = 2[V_O^{\cdot\cdot}]$. Since we assume $[A'] \gg [e']$ we obtain:

$$D^{\delta} \approx \frac{2D_{V_O^{\cdot\cdot}}[A']}{[e']} = D_{V_O^{\cdot\cdot}} \sqrt{\frac{2[A']^3}{K_O}} p(O_2)^{1/4}. \quad (12)$$

Since $[A'] \gg [e']$ we find that D^{δ} must be larger than $D_{V_O^{\cdot\cdot}}$ and now depends on $p(O_2)$.

(iv) *Strong trapping by deep dopants* : We assume that almost all electrons are trapped by one or several types of dopants. In the case of a single dopant we can write $K_{T_1}[T_1] \gg [e']$. We then obtain for the chemical diffusion coefficient:

$$D^{\delta} \approx D_{V_O^{\cdot\cdot}}. \quad (13)$$

The only limiting case in which a $p(O_2)$ dependence results and $D^{\delta} \gg D_{V_O^{\cdot\cdot}}$ holds is the case of compensation by a fixed valence acceptor, in the other cases considered D^{δ} is $p(O_2)$-independent and close to $D_{V_O^{\cdot\cdot}}$. This finding will be of special relevance for the discussion of the results for the dependence of the chemical diffusion coefficient on oxygen partial pressure and dopant content.

2. Experimental

2.1. Sample preparation and control of oxygen partial pressures

Some of the SnO_2 crystals were kindly supplied by R. Helbig (University of Erlangen). They were grown by vapour phase transport in an hydrogen-containing atmosphere [14]. Though nominally undoped, they contained traces especially of iron and aluminum and will be referred to as "weakly iron-doped crystals". Brown, strongly iron-doped samples were obtained by a gas-phase reaction method [19] from tin metal in a special crucible which allows for slow oxygen in-diffusion and which is placed in a temperature gradient ($T_{max} = 1320\,^{\circ}C$). The iron doping was achieved by adding some Fe_2O_3 into the crucible. The same method was utilized for chromium-doped crystals (intense purple colour). Manganese-doped samples were prepared from weakly iron-doped singles crystals by cation diffusion. The crystals were embedded in MnO and kept for 14 days at 1200°C in a flowing N_2 atmosphere ($p(O_2) \approx 10^{-4}$ atm). Since manganese introduces a yellow colour, optical microscopy was used to check whether the manganese content was distributed homogenously in the sample.

Single-crystallinity was checked by applying the Laue diffraction method to different spots of the sample. After cutting the crystals in the desired orientation, they were deliberately not fine-polished to keep the surface active for oxygen exchange. The quantitative determination of dopant concentrations was difficult owing to the low contents, and only ICP-AES (Pascher Analytik, Remagen, Germany) was sufficiently sensitive. The results are given in Table 1. All samples were predominantly acceptor doped, as supported by conductivity experiments.

Table 1
Impurity contents in SnO_2 single crystals

Batch	$[Al]_0$	$[Ca]_0$	$[Fe]_0$	$[Mn]_0$	$[Si]_0$	
Z-30	4×10^{-5}	8×10^{-6}	8×10^{-5}	3×10^{-6}	1×10^{-4}	Weakly iron doped
Z-34	1×10^{-5}	1×10^{-5}	5×10^{-5}	3×10^{-6}	5×10^{-5}	Weakly iron doped
Mn-I	6×10^{-5}	1×10^{-5}	6×10^{-5}	5×10^{-5}	4×10^{-5}	Manganese doped
Fe-4	2×10^{-5}	4×10^{-6}	5×10^{-4}	$<3\times10^{-6}$	4×10^{-3}	Iron doped

Concentrations are given as mol(impurity)/mol(Sn).

Oxygen partial pressures were adjusted using O_2/N_2 mixtures for $p(O_2)$ down to 10^{-5} atm and mixtures of CO and CO_2 in Ar for lower $p(O_2)$. In CO/CO_2 atmospheres, the surface exchange reaction becomes rate-determining for the stoichiometry change kinetics at temperatures below $\approx$ 800 °C. This could be avoided by using a catalyst: A very thin layer of platinum (20 nm) was sputtered onto all large sides of the samples. During subsequent annealing (800 C, 15 h) the film agglomerated into small isolated islands (diameter-$\approx$0.2 μm) which did not interfere with the EPR or conductivity measurements, since no conducting pathways were formed.

2.2. Conductivity relaxation experiments

Single crystals of SnO_2 were exposed to sudden changes in $p(O_2)$ while the overall conductivity change was measured in situ using a four-point DC method (for details see [15]). The experiments were performed on the weakly iron-doped samples from the hydrogen transport method. A rod-shaped sample (6.5 mm × 1.9 mm × 1.9 mm) and a plate-shaped sample (5.0 mm × 2.0 mm × 0.3 mm) were used.

2.3. EPR relaxation experiments

Ex situ EPR relaxation experiments were performed using a Bruker EMX spectrometer (X-band) with goniometer. After changes in $p(O_2)$, the time-dependent response of the EPR signal of Fe'_{Sn} or Mn^x_{Sn} was recorded. For this, samples were annealed for defined time intervals and rapidly quenched to room temperature. The Fe'_{Sn} signal was identified by its angular dependence in the *c*-plane and by comparison with the literature [11]. The spectra were recorded with the field perpendicular to the (110)-plane, and the strongest signal at a magnetic field of 1950 Gauss was analyzed. For manganese, X-band measurements were not available in the literature. However, by their characteristic hyperfine splitting into six lines, two signal groups could be easily assigned to manganese, and the characteristic angular dependence indicated that the respective manganese ion occupies a tin position. According to Kramers' theorem the signal could originate from Mn^{2+}, Mn^{4+} or Mn^{6+}. It was observed that the signal disappears on reduction of the sample. As the presence of Mn^{+} can be discarded [16], the relevance of the redox pair Mn^{+}/Mn^{2+} can be excluded. Mn^{4+} and Mn^{3+} match the ionic radius of Sn^{4+} better than Mn^{6+} and Mn^{5+} [17]. Additionally, defects with a low net charge tend to be more stable than defects with higher charges. Therefore it was concluded that the signal originates from Mn^{4+} occupying tin positions in the lattice (Mn^x_{Sn}).

Intensities I_{av} were obtained by averaging the double integral and the peak-to-peak intensity of the EPR signal. From measurements at different microwave powers, it was assured that the signal was not saturated. A piece of iron-doped $SrTiO_3$ ceramics was used as a standard to compensate for changes in the quality factor of the cavity which are caused by changes in the sample conductivity. The intensities I were finally normalized according to:

$$I = \frac{I_{av}/I_{av,std}}{I^{ox}_{av}/I^{ox}_{av,std}}. \tag{14}$$

The subscript std denotes "standard" (Fe-doped $SrTiO_3$, see above) and the superscript ox denotes the fully oxidized sample (all iron present as Fe^{3+} or all manganese present as Mn^{4+}, respectively).

To ensure that the signal intensity was not influenced by the skin effect, the conductivity σ of a strongly reduced sample ($I = 12\%$) was measured using the four-point-DC method yielding $\sigma = 3.0\times10^{-3}\,\Omega^{-1}\,cm^{-1}$. The corresponding penetration depth (6.5 mm) was greater than the sample half-thickness ($l = 0.15$ mm). Additionally, a plate-shaped sample was reduced in size by polishing off the large surface to check that the intensity was proportional to the sample mass and not to the sample surface area.

The chemical diffusion coefficients of oxygen in SnO_2 were obtained from the time-dependent response of the EPR or conductivity signal by means of a non-linear least-squares regression (for details see [15]).

3. Results and discussion

3.1. Conductivity relaxation experiments

The time dependence of the conductivity signal in the relaxation experiments was found to be far more complicated than expected. Instead of one relaxation process which can be attributed to the oxygen stoichiometry change of the bulk of the sample, three processes were found. Fig. 1 shows a representative measurement performed on the rod-shaped sample at 800 °C. Fig. 1a focusses on the process with the shortest time constant. The change of conductivity was observed to be so fast

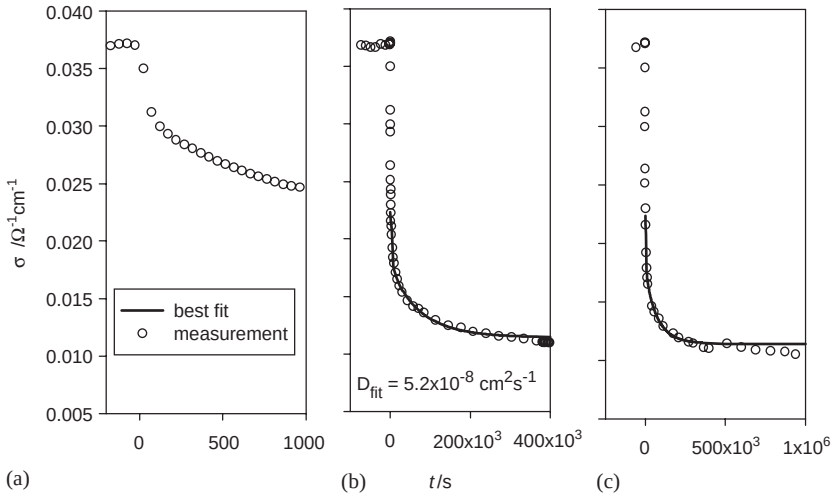

Fig. 1. Conductivity relaxation experiment on a weakly iron-doped sample (rod shaped, 6.5 mm × 1.9 mm × 1.9 mm, $p(O_2)$: 0.05 atm → 1 atm, 800 °C). The line indicates the fit yielding D^{δ}.

that it could not be distinguished from the gas residence time of the experimental set-up. The magnitude of the conductivity change for this process was irreproducible. A relative change in conductivity could be computed for this process when the change in conductivity was divided by the initial conductivity observed before the change in $p(O_2)$. When averaged values (from several $p(O_2)$ changes) for the thicker, rod-shaped sample and for the thinner, plate-shaped sample were compared, it was found that this average was much larger for the thin sample. At least for the rod-shaped sample the change in conductivity was generally smaller than the change expected from the oxygen exchange equilibrium (Eq. (5)). These observations indicated that this first process could not be attributed to a bulk stoichiometry change. The speed of the process and its dependence on sample thickness point towards a surface process, i.e. to the conductivity change of a highly conductive surface layer.

The second process is much slower than the first: At the temperature of 800 °C it has decayed after about 300×10^3 s as can be seen in Fig. 1. Using Eq. (5) the exponent of the $p(O_2)$ dependency was computed to $n = 0.19$ which is in between the values of 1/6 or 1/4 expected from the standard defect chemical model for the limiting cases given in Eq. (5) cases (i) and (ii). This already suggests the second process to be the chemical diffusion of oxygen. This can be further supported by comparing the time dependencies of the conductivity relaxation during the second process for different sample thicknesses. As shown in [15] these time dependencies become invariant of sample thickness $2l$ when the conductivities are plotted against time divided by the square of the sample half-thickness t/l^2. This dependence on t/l^2 is a typical feature of diffusion processes [18] and shows also that the kinetics of the stoichiometry change is not limited by the surface exchange reaction but by the chemical diffusion of oxygen.

The almost linear decline in conductivity which can be seen between 500×10^3 s and 1000×10^3 s in Fig. 1 indicates a third process. At 800 °C the third process is so slow that it could not be followed sufficiently long to observe equilibration. Note that the conductivity change resulting from the third process has the same tendency as the changes resulting from the two preceding processes. This implies that the overall conductivity change resulting from all processes (or from the sum of the second and third process) is larger than expected from the oxygen exchange equilibrium alone. At 900 °C the relaxation time of the third process is on the order of days which makes the observation of its equilibration feasible. This can be seen in two relaxation experiments in Fig. 2. Owing to the scaling of the graph only the third process is resolved. The arrows indicate the conductivity change expected after the $p(O_2)$ change from the standard defect model using an exponent of $n = 1/4$ (the base of the arrow starts at the conductivity observed after the first process has approximately equilibrated). Like in the measurement at 800 °C, the overall change in conductivity is significantly larger than expected from the oxygen exchange equilibrium alone (see Eq. (5)). The time-dependence of the conductivity is irregular to some degree (see e.g. the "steps" at 2.2×10^6 s or at 4.2×10^6 s occuring without $p(O_2)$ or T change) as will be discussed in Section 3.7.

3.2. Additional experiments on the nature of the third relaxation process

The long-time conductivity changes due to the third process are induced not only by changes in oxygen partial pressure but also by temperature changes. This

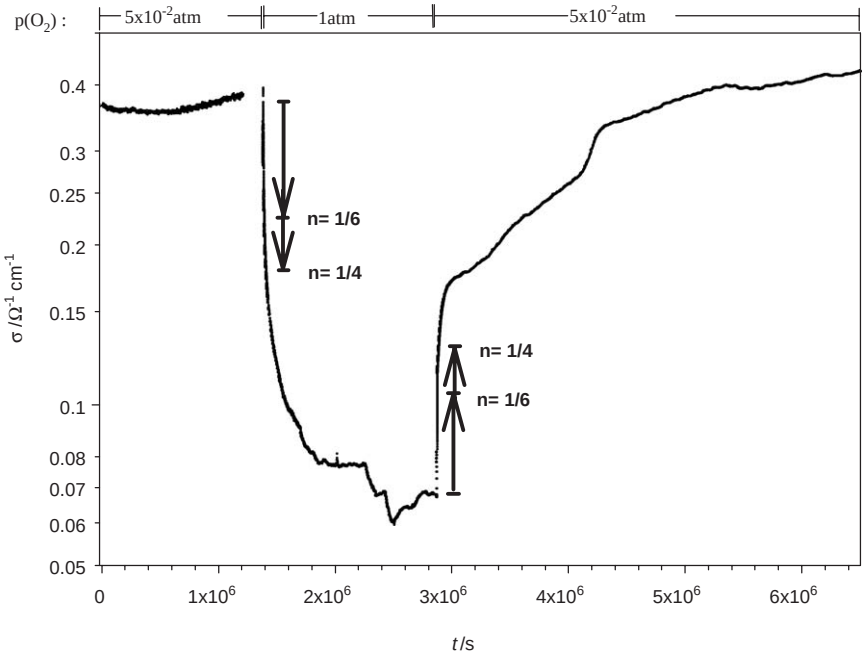

Fig. 2. Conductivity relaxation experiments on a weakly iron-doped sample at 900 °C. Also indicated are the oxygen partial pressures. The arrows show the conductivity changes that would be expected from Eq. (5). Please note the logarithmic scaling on the conductivity axis.

was confirmed when a sample was first annealed in air at 1100 °C for 7 days. It was then brought into pure O_2 at 800 °C long enough to equilibrate the first and second relaxation processes. After this, the conductivity was $3.6 \times 10^{-4}\,\Omega^{-1}\,cm^{-1}$. Then the sample was annealed at 1300 °C in air for two days. Its conductivity at 800 °C in pure O_2 was again measured after equilibration of the second process, resulting in a value of $7.7 \times 10^{-4}\,\Omega^{-1}\,cm^{-1}$. Since the enthalpy of the oxygen exchange reaction (Eq. (1)) is positive [8], an increase in temperature will lead to a reduction of the tin dioxide. Both the reduction of SnO_2 by means of a $p(O_2)$ decrease or a temperature increase change the conductivity in the same direction. Apparently the third process is initiated by a reduction (or oxidation) of the sample in general. If the third process can be attributed to some bulk defect chemical origin, it leads to an additional increase in the electron concentration when the sample is reduced; or to the respective decrease upon oxidation.

Conductivity relaxation experiments were also performed on a weakly iron-doped sample grown with the gas-phase reaction method according to Reed et al. [19]. This was done to support that the observations described above reflect a genuine property of acceptor-doped SnO_2, and are not unique to the specific samples obtained from the hydrogen transport method (Thiel and Helbig [14]). In these experiments the additional slow process could be reproduced [20]. These observations will also be interpreted in Section 3.7.

3.3. EPR relaxation experiments

Since the results of the conductivity experiments were rather complex and difficult to interpret, EPR relaxation was utilized (i) as an independent method to confirm that the second process can indeed be attributed to chemical diffusion of oxygen, and (ii) to derive D^{δ} more reliably. The experiments were performed on the manganese-doped, iron-doped and weakly iron-doped samples. In addition to the process attributed to chemical diffusion of oxygen, a slower process was found. Since changes in the EPR signal can only be observed in a relatively narrow range of oxygen partial pressures, it was very difficult to follow the time dependence of the slow process directly. The signal would either fall below the detection limit or be saturated according to Eq. (6b). However, it is very instructive to monitor the $p(O_2)$ dependence of the EPR signals for different reducing or oxidizing pretreatments when the slow process is "frozen in" (allowing just enough time ≈ 1 h for the oxygen stoichiometry to equilibrate, i.e. for the chemical diffusion process to relax).

Fig. 3a shows such a measurement for a manganese-doped sample. The crystal was first pretreated under oxidizing conditions (5 d, 850 °C, in air) for a prolonged period of time and then the $p(O_2)$ dependence of the Mn_{Sn}^{x} signal was recorded. After that the crystal was pretreated under reducing conditions (5 d, 850 °C, $p(O_2) = 1.6 \times 10^{-13}$ atm) and the $p(O_2)$ dependence

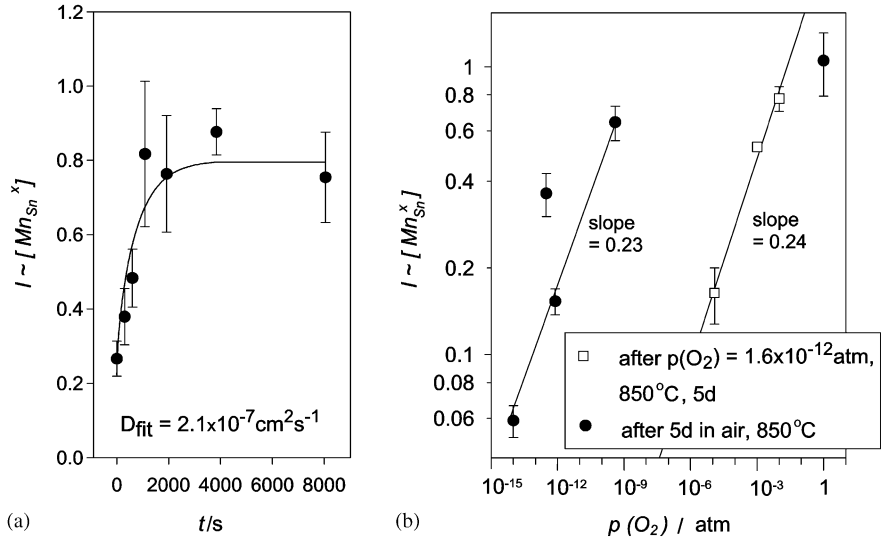

Fig. 3. (a) EPR relaxation experiment on a manganese-doped sample (rod shaped, 0.85 mm × 0.85 mm × 3.4 mm, $p(O_2)$: 1.7×10^{-13} atm → 1.3×10^{-11} atm, 800 °C). (b) Partial pressure dependence of the Mn_{Sn}^{x} signal in a manganese-doped sample measured after prolonged pretreatment under reducing and oxidizing conditions.

recorded again. The reducing pretreatment led to a shift in the straight line describing the $p(O_2)$ dependence to higher values, i.e. manganese can already be reduced at higher $p(O_2)$). That means that the reducing pretreatment has led to a persistent increase in the sample's electron concentration and hence in the Fermi level. Annealing under oxidizing conditions has the opposite effect. It is thus very reasonable to assume that the third process in the conductivity experiments is identical with the slow process in the EPR experiments. Apart from the dependence on the pretreatment, the Mn_{Sn}^{x} signal changes with $p(O_2)$ with an exponent of 0.23 or 0.24 which agrees very well with the value of 1/4 expected from Eq. (6a) case (ii). The dependence on the pretreatment was also observed for the weakly iron-doped crystal [15]. It is important to note that the EPR method produces a signal to which the whole sample volume contributes. We thus conclude that the third process results from a complication in the bulk defect chemistry of SnO_2. From the conductivity results alone this could not be concluded since other effects such as a slow change in the surface conductivity could also have led to such observations.

3.4. Dependence of the chemical diffusion coefficient of oxygen on temperature, sample composition and orientation

Fig. 4 summarizes the results for the chemical diffusion coefficient of oxygen in SnO_2 determined with differently doped samples from conductivity (second process) as well as EPR experiments. The activation energy E_A and pre-exponential factor D_0 were obtained from linear regression on a $\ln(D^{\delta})$ vs $1/T$-plot. Table 2 summarizes these results. The difference beween the differently doped samples was not found to be significant. Thus the results were assumed to belong to one data collective and D^{δ} was determined from a fit of all data points:

$$D^{\delta} = D_0 \exp\left(-\frac{E_A}{kT}\right) \tag{15}$$

with $D_O = \exp(-4 \pm 2)\,cm^2\,s^{-1}$, $E_A = (1.1 \pm 0.3)\,eV$.

As shown previously [15], the orientation dependence of D^{δ} was not found to be significant.

The chemical diffusion coefficients measured in this work are consistent with reports by Samson and Fonstad [5] who report conductivity equilibration times for SnO_2 single crystals after $p(O_2)$ changes at 1100 °C. $D^{\delta} \approx 10^{-5}\,cm^2/s$ can be derived from [5] which is comparable to the value of $2 \times 10^{-6}\,cm^2/s$ calculated from Eq. (15). In the literature, two more sets of diffusion coefficients are reported. Maier and Göpel [3] measured diffusion coefficients on pressed powders (grain size ≈ 1 μm) of SnO_2. Hellmich et al. [4] deduced D^{δ} from the kinetics of the oxidation process of small (≈ 1 μm) tin spheres. Their results conflict with the results reported by Maier and Göpel as well as the results of this work. It is worth noting that both Maier and Göpel as well as Hellmich et al. report lower diffusion coeffients but higher activation enthalpies E_A. The most likely interpretation for theses discrepancies is that the surface exchange reaction was limiting instead of chemical diffusion in these studies. This is supported by the fact that the particle sizes in both cases are much smaller than the single crystals used in this work, and small particle sizes (i.e. small diffusion lengths) favour a limitation by surface exchange [21].

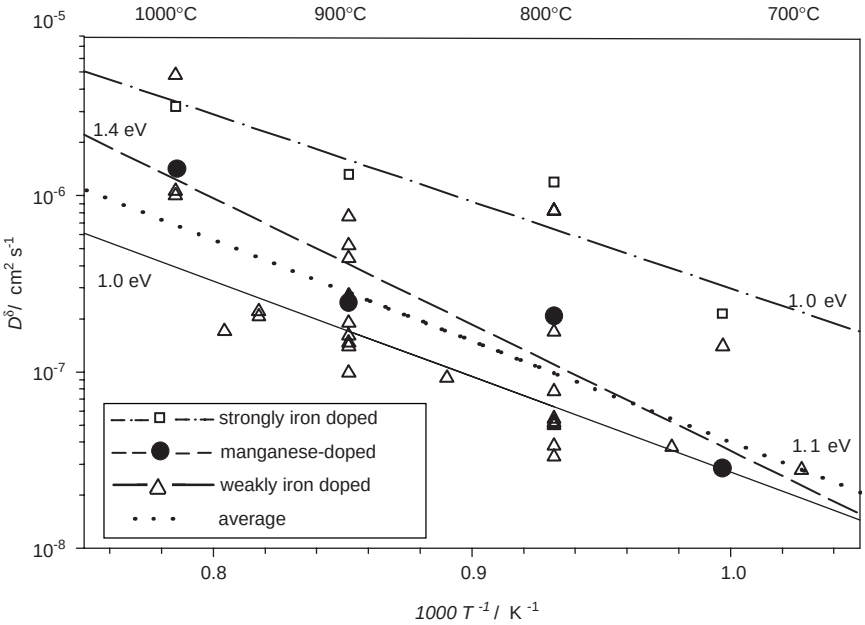

Fig. 4. Temperature dependence of chemical diffusion coefficients for different dopant contents.

Table 2
Temperature dependence of the chemical diffusion coefficient for different dopant contents and experimental methods

Dopant	Method	E_A/eV	$\ln(D_0/\mathrm{cm^2\,s^{-1}})$
Weakly iron doped	Conductivity, rod shaped	1.4±0.3	−2.0±3.5
Weakly iron doped	Conductivity, plate shaped	0.8±0.1	−7.9±1.4
Weakly iron doped	EPR	0.9±0.4	−5.5±3.6
Manganese doped	EPR	1.4±0.3	−6.6±3.5
Strongly iron doped	EPR	1.0±0.3	−3.7±2.9
Common fit of all data		1.1±0.3	−4±2

3.5. Equilibrium constants of trapping reactions

For simulations of the $p(O_2)$ dependence of the chemical diffusion coefficients, equilibrium constants of trapping reactions were needed. They were determined with a combination of EPR and conductivity experiments for a temperature of 800 °C. The concentration ratio of the oxidized and reduced forms of the respective dopant was measured by EPR. For the example of iron we obtain:

$$\frac{[\mathrm{Fe}'_{\mathrm{Sn}}]}{[\mathrm{Fe}''_{\mathrm{Sn}}]} = \frac{I}{1-I}. \tag{16}$$

The electron concentration was determined from the conductivity according to

$$[\mathrm{e}'] = \frac{\sigma}{u_{\mathrm{e}'}\mathrm{e}}. \tag{17}$$

The electron drift mobility $u_{e'}$, extrapolated to 800 °C with the respective temperature dependence, was taken from Hall experiments reported by van Daal [22] (21.2 $\mathrm{cm^2\,V^{-1}\,s^{-1}}$) as well as Fonstadt and Rediker [25] (20.3 $\mathrm{cm^2\,V^{-1}\,s^{-1}}$) and averaged to a value of 20.8 $\mathrm{cm^2\,V^{-1}\,s^{-1}}$. The impurity concentrations of the samples used in this work are roughly the same as those reported in the literature. Following [25] a value of 1.18:1 was used as the ratio of Hall- and drift-mobility. Insertion of the results from Eqs. (16) and (17) into Eq. (3b) yields the equilibrium constants. An effective electron mass $m^* = 2.9m_e$ averaged from [22–25] allows to calculate the effective density of states. Thus the standard free enthalpy of the respective trapping reaction, i.e. the distance of the respective level to the lower edge of the conduction band can be obtained. These results are summarized in Fig. 5.

3.6. Dependence of the chemical diffusion coefficient on oxygen partial pressure

Fig. 6 shows the dependence of the chemical diffusion coefficient on the average electron concentration [e′] in the material, which is the relevant electronic charge carrier affecting D^{δ}. A plot of D^{δ} versus $p(O_2)$ is not feasible here, because the incomplete third relaxation process induces a persistent shift in the Fermi level i.e. electron concentration, which therefore depends not

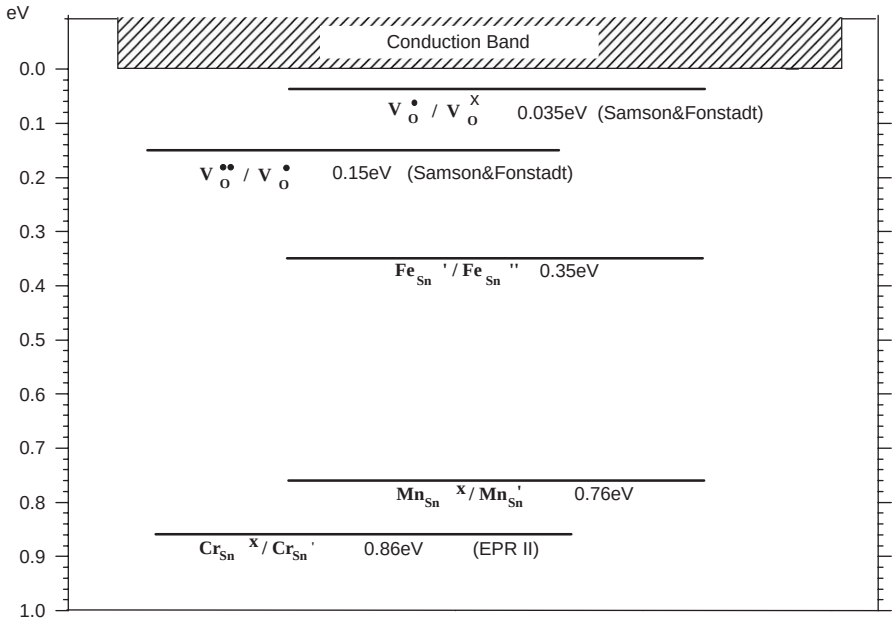

Fig. 5. Location of deep donor levels in the band gap. Also shown are the donor levels of oxygen vacancies reperted by Samson and Fonstad [5]. The Cr_{Sn}^{x}/Cr_{Sn}'-level refers to the center designated EPRII by Hikita et al. [34].

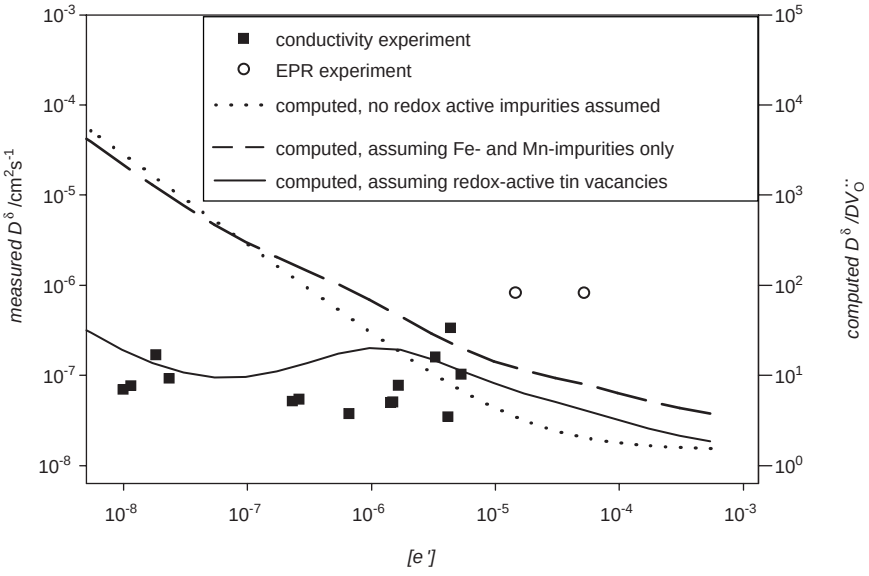

Fig. 6. Dependence of the experimentally determined chemical diffusion coefficient D^{δ} on the electron concentration at 800 °C (weakly Fe-doped sample). Superimposed are ratios of the chemical to the oxygen vacancy diffusion coefficient computed with Eq. (7). The observed D^{δ} is independent of the electron concentration. This cannot be explained by the redox-active dopants found in the chemical analysis. Under the assumption that redox-active tin vacancies are present the ratio $D^{\delta}/D_{V_O^{\cdot\cdot}}$ is computed to be independent of the electron concentration (assumptions: $[V_{Sn}] = 5 \times 10^{-5}$ mol/mol Sn, $K_{TS} = 10^{-7}$ mol/mol Sn).

only on $p(O_2)$ but also on pretreatment. The electron concentration was determined by averaging the conductivities measured before and after the relaxation experiments (performed at various $p(O_2)$) and subsequent conversion according to Eq. (17). In Fig. 6 , ratios $D^{\delta}/D_{V_O^{\cdot\cdot}}$ computed from Eq. (7) for different defect models are also shown, which can be compared to the experimentally observed dependence of D^{δ} on the electron concentration. The oxygen vacancy concentration was obtained from the electroneutrality condition (Eq. (4)) using the mass action laws for the trapping equilibria to determine the concentrations of the respective species. Three cases were considered:

- No redox-active species are present.
- The redox-active species iron and manganese have concentrations as obtained from chemical analysis (see Table 1).

- Along with iron and manganese an additional trap is present. A concentration of 5×10^{-7} mol/mol Sn and an equilibrium constant of $K_{TS} = 10^{-7}$ mol/mol Sn were arbitrarily assumed for this trap.

The measured diffusion coefficients are independent of the electron concentration. The computational results demonstrate that this would not be expected if only the concentrations of redox-active species from the chemical analysis were involved. However, if an additional trap is present, the experimental observation can be explained. In Section 3.7 we propose that redox-active, non-fully ionized tin vacancies exist in the material which could act as additional traps.

The independence of the observed oxygen chemical diffusion coefficient from the electron concentration allows us to conclude that the chemical diffusion coefficient measured in this work is close to the diffusion coefficient of oxygen vacancies. This can be deduced from the defect-chemical derivation in Section 1.3 (cases i–iv). While the acceptor-doped case (case iii) forces the chemical diffusion coefficient to vary with the electron concentration, all other possible cases yield $D^{\delta} = D_{V_O^{\bullet\bullet}}$ or $D^{\delta} = 3D_{V_O^{\bullet\bullet}}$. The conclusion is also supported by the observation that the chemical diffusion coefficient does not change significantly when the dopant content of the samples is varied: For a sample doped with a redox-active acceptor, an increase in dopant concentration leads to a decrease in the chemical diffusion coefficient by decreasing χ (see Eq. (9)), provided the material is not already in the "strong trapping" regime (see Eq. (13)). It is however observed that for the "strongly iron-doped" or "manganese-doped" samples the chemical diffusion coefficient does not change significantly compared to the diffusion coefficients of "weakly iron-doped" samples. This indicates that the weakly iron-doped samples already *are* in the "strong trapping" regime, meaning that the chemical diffusion coefficient is close to that of oxygen vacancies $D_{V_O^{\bullet\bullet}}$ according to Eq. (13). It also implies that for any SnO_2 crystals with other dopant contents (i.e. different concentration and/or type) than the ones used in this work, the chemical diffusion coefficients can only be close to or higher than the values measured in this work.

3.7. Interpretation of the additional slow process observed in relaxation experiments

In the following, we suggest a model to explain the additional process that was observed to relax much slower than chemical diffusion of oxygen. In Section 3.3 it was concluded that this process is due to a complication in the bulk defect chemistry.

Tin interstitials $Sn_i^{\bullet\bullet\bullet\bullet}$ ($SnO_2 \rightleftharpoons O_2 + Sn_i^{\bullet\bullet\bullet\bullet} + 4e'$) have previously [3,8] been excluded as predominant native defects in SnO_2 because the expected exponent $n = 1/5$ of the $p(O_2)$ dependence of defect concentration was not observed. Also in this work the assumption of $Sn_i^{\bullet\bullet\bullet\bullet}$ is not consistent with the experimental data. If $Sn_i^{\bullet\bullet\bullet\bullet}$ (instead of $V_O^{\bullet\bullet}$) were the dominant defect species and therefore also the species predominantly transported, there would be no additional species to explain the slow relaxation. If $Sn_i^{\bullet\bullet\bullet\bullet}$ and $V_O^{\bullet\bullet}$ were present in comparable amounts, the predicted $p(O_2)$ dependence of [e′] for full equilibration would be between $-1/5$ and $-1/6$ (case of negligible acceptor concentration), or $-1/4$ (acceptor-doped case). The magnitude of these exponents is significantly smaller than the observed value (see Fig. 2).

Another complication in the defect chemistry of SnO_2 would be the occurrence of associated species, e.g. involving oxygen vacancies and the acceptor defect $(V_OA)^{\bullet}$. The time constant of the association process would require transport only over the short distances between the defects (a few lattice constants) and thus cannot explain the slow process.

Schottky defects (which must be formed at high temperatures according to thermodynamics) would produce highly charged tin vacancies $V_{Sn}^{''''}$ [10]. It is likely that these will release electrons according to

$$V_{Sn}^{''''} \rightleftharpoons V_{Sn}^{'''''} + e', \tag{18a}$$

thus reducing their charge (this can be regarded as the release of an electron from one of the neighbouring oxide ions). For the mass action constant K_{TS} of reaction (18a) we obtain

$$K_{TS} = \frac{[V_{Sn}^{'''''}][e']}{[V_{Sn}^{''''}]}. \tag{18b}$$

Equilibration assumed, the tin vacancy concentration $[V_{Sn}^{''''}]$ obeys the mass action law for the Schottky equilibrium (2) and also couples to the oxygen exchange equilibrium (1). Assuming further that triply charged tin vacancies dominate the electroneutrality condition ($3[V_{Sn}^{'''''}] = 2[V_O^{\bullet\bullet}]$) we obtain for the $p(O_2)$ dependence of the electron concentration

$$[e'] = \sqrt[5]{\frac{2K_O^3}{3K_S K_{TS}}}\, p(O_2)^{-3/10}, \tag{19}$$

while we get

$$[e'] = \left(\frac{2K_O^3}{(4-v)K_S K_{TS}}\right)^{1/(6-v)} p(O_2)^{-3/(12-2v)}, \tag{20}$$

if the charge of the tin vacancies is $4 - v$. Eq. (20) describes the partial pressure dependence of the electron concentration that would be observed if both the oxygen exchange reaction (1) and the Schottky reaction (2) have equilibrated. The resulting exponent of the partial pressure dependence exceeds the maximum value of 1/4 that would be expected for a change in oxygen

stoichiometry alone. This agrees with observations both in EPR and conductivity experiments (in Fig. 2 the sum of all processes yields an exponent $\approx 1/2$).

If on the other hand, the Schottky equilibrium is frozen, while the oxygen exchange reaction (1) is allowed to equilibrate, we obtain from the oxygen exchange equilibrium (1b) and the electroneutrality condition $3[V'''_{Sn}]_F = 2[V^{\bullet\bullet}_O]$:

$$[e'] = \sqrt{\frac{2K_O}{3[V'''_{Sn}]_F}} p(O_2)^{-1/4}, \tag{21}$$

where $[V'''_{Sn}]_F$ is the constant concentration of Schottky vacancies. This $p(O_2)$ dependence of the electron concentration cannot be distinguished from the one expected for the acceptor-doped case (Eq. (5), case ii), in agreement with the observations from conductivity (Section 3.1) and EPR experiments (Fig. 3b). When the slow relaxation process is frozen, the partial pressure dependence of the EPR and conductivity signal follows a 1/4-dependence as expected from Eq. (5).

The model involving Schottky defects is also consistent with the additional process being slower than the chemical diffusion of oxygen. It is not unreasonable to assume that the necessary diffusion of highly charged tin vacancies is slower than the diffusion of oxygen vacancies. Thus the Schottky reaction would proceed slower than the oxygen incorporation. The "irregular" conductivity changes in Fig. 2 can also be explained by partially ionized Schottky defects: The coupling between the sublimation equilibrium $SnO_{2,surf} \rightleftharpoons SnO_{gas} + \frac{1}{2}O_2$ and the Schottky equilibrium (Eq. (2)) finally leads to a dependence of the electron concentration on the SnO partial pressure which is not well defined under the experimental conditions [20].

It is worth mentioning that Yoo and coworkers [26] have also observed twofold kinetics in experiments on donor-doped $BaTiO_3$ in a certain $p(O_2)$ range. After a change in $p(O_2)$, two relaxation processes were observed on different time scales. One of these is believed to be related to the diffusion of oxygen vacancies, the other to the much slower diffusion of cations (but in contrast to the current study, no additional trapping equilibrium was involved).

3.8. Drift of Taguchi sensors

In the following the relevance of the results for drift processes in Taguchi sensors will be discussed. As was mentioned in Section 3.6 the chemical diffusion coefficients obtained in this work represent a lower limit to the values observed in materials with different dopant contents. Thus for a Taguchi sensor, an upper limit for the characteristic decay time τ of the drift process can be estimated if oxygen diffusion is presumed to be rate-determining. The characteristic time can be roughly estimated by

$$\tau = \frac{L^2}{D(T)}, \tag{22}$$

where L is the characteristic length of the diffusion path. For a Taguchi sensor L may be the radius of a SnO_2 grain (then D^δ is the relevant diffusion coefficient) or the thickness of the electron-depleted surface layer of the grains (redistribution of $V^{\bullet\bullet}_O$ within the space charge layer, then the vacancy mobility $\propto D_{V^{\bullet\bullet}_O}$ is the relevant kinetic quantity). In Fig. 7 characteristic times computed using Eq. (22) and $D^\delta(T)$ from Eq. (15) are compared with characteristic times observed for drift processes on actual sensors [27–29]. It can be seen that the characteristic times computed from $D^\delta(T)$ are much shorter than those observed on actual sensors. This leads to the conclusion that not the chemical diffusion, but the surface exchange reaction is the rate-determining step of the overall reaction of stoichiometry change leading to signal drift.

The surface exchange reaction itself is composed of various steps. Using studies of the surface chemistry of oxygen on SnO_2 from the literature, it is possible to suggest the most likely path of oxygen incorporation and to narrow down the rate determing step. It is reported [30,31] that oxygen chemisorbs as O_2^- and O^- on SnO_2. From this the most likely mechanism for the oxygen in- or excorporation can be deduced:

$$O_{2,\,gas} \rightleftharpoons O_{2,\,adsorbed}, \tag{23}$$

$$O_{2,\,adsorbed} + e^- \rightleftharpoons O^-_{2,\,adsorbed}, \tag{24}$$

$$O^-_{2,\,adsorbed} + e^- \rightleftharpoons 2O^-_{adsorbed}, \tag{25}$$

$$O^-_{adsorbed} + e^- \rightleftharpoons O^{2-}_{1.\,bulk\ layer}. \tag{26}$$

The last reaction comprises the incorporation of adsorbed O^- into the bulk (ionic transfer) as well as an electron transfer, but the observations available here do not allow to draw conclusions if those two processes occur simultaneously or consecutively. On sintered pellets of SnO_2 Blaustein et al. [27] noticed a fast initial response of the conductivity to a change in oxygen partial pressure which was followed by slow drift processes. The fast initial response indicates that the steps up to and including the first electron transfer (Eq. (24)) cannot be rate-determining for the overall reaction. This is also supported by chemisorption rates reported by Sberveglieri et al. [32]. The sensor's response to carbon monoxide is mainly caused by the following reaction [31,33]:

$$CO_{adsorbed} + O^-_{adsorbed} \rightleftharpoons CO_2 + e^-. \tag{27}$$

The signal recovery after a CO exposure is faster than the drift processes (see for example Fig. 3 in [28]). This indicates the reequilibration of the concentration of

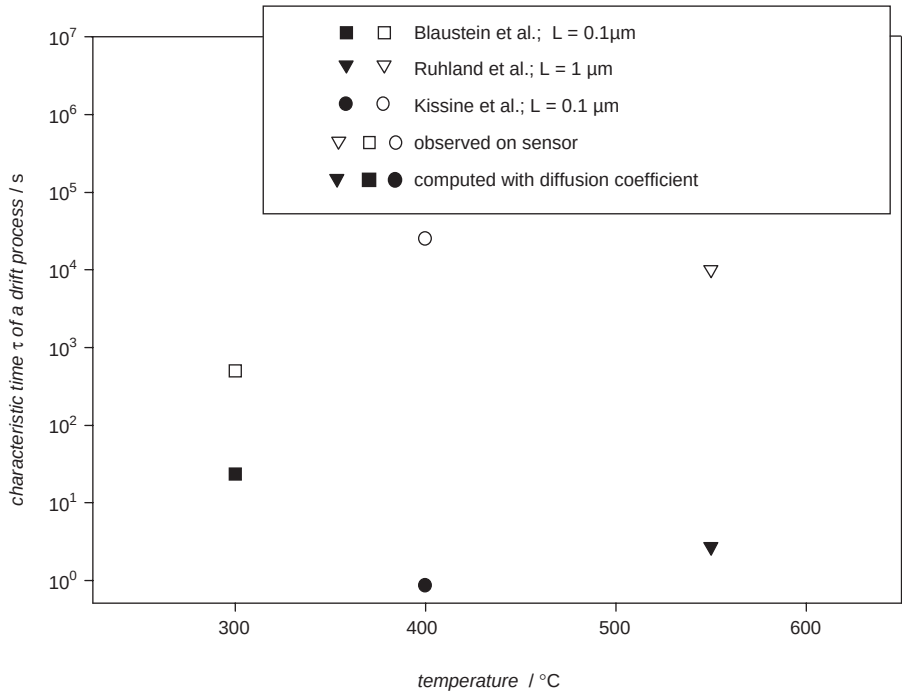

Fig. 7. Comparison of characteristic times for drift processes of Taguchi sensors. Full symbols indicate characteristic times computed under the assumption that bulk chemical diffusion of oxygen is rate-determining. Open symbols indicate characteristic times of drift processes observed on sensors by various authors [27–29]. The computed values are much shorter than the observed values, indicating that the surface reaction is rate-determining for the kinetics of drift processes. Please note that the approximate diffusion lengths L (i.e. grain radii) are not the same for all publications. Also note that from the publications of Kissine et al. and Ruhland et al. lower limits for the characteristic times are shown.

adsorbed O^- to be faster than the rate determinining step of the drift process. If this reequilibration occured via Eq. (26) it would result in an irreversible reduction of the bulk tin oxide, which would induce tremendous drift effects and render the device unusable. From that we conclude that the reequilibration of the adsorbed O^- occurs via reaction (25). This means that at least the forward path of the latter reaction cannot be rate-determining either. Thus the incorpration of adsorbed O^- together with the last electron transfer (Eq. (26)) is supposed to be rate-determining for the drift processes.

4. Summary

Chemical diffusion coefficients for oxygen in tin dioxide were measured with two independent methods (EPR- and conductivity-relaxation) on single crystals. The temperature dependence of the chemical diffusion coefficient was found to be

$$D^{\delta} = \exp(-4 \pm 2)\,\mathrm{cm^2\,s^{-1}}\ \exp(-(1.1 \pm 0.3)\,\mathrm{eV}/kT).$$

No significant dependence on oxygen partial pressure or dopant content was observed. This indicates that the chemical diffusion coefficients measured in this work are the lower limits to the values that will be found in other samples with different dopant content (type and/or concentration). The results of the relaxation experiments were influenced not only by the oxygen stoichiometry change alone but also by additional processes occurring on different time scales. A process slower than chemical diffusion of oxygen was found both in conductivity and EPR measurements. The observation of this process in the EPR measurements proves that the process is due to a complication in the bulk defect chemistry of the material.

As cause for an additional slower relaxation process the following was suggested: Tin vacancies V_{Sn}'''' which are formed by the Schottky reaction can act as electron donors according to $V_{Sn}'''' \rightleftharpoons V_{Sn}^{(4-v)'} + ve'$. The Schottky reaction thus influences the concentration of electrons. Defect models based on this assumption yield a stronger oxygen partial pressure dependence of the conductivity than models neglecting partial ionization of Schotty defects. This is in agreement with experimental observations from conductivity and EPR experiments. Additional observations support this explanation: The independence of the chemical diffusion coefficient on oxygen partial pressure indicates that along with the transition metals observed in chemical analysis, additional traps for electrons are present. Changes in the conductivity during the third relaxation process can be explained with the coupling between the Schottky reaction and the sublimation reaction.

Using a combination of EPR and conductivity measurements, equilibrium constants and standard free enthalpies of trapping reactions could be computed for relevant transitions metal dopants. The following standard free enthalpies (i.e. distance between the respective levels and the conduction band) were obtained: Fe'_{Sn}/Fe''_{Sn}: 0.35 eV; Mn^{x}_{Sn}/Mn'_{Sn}: 0.76 eV; Cr^{x}_{Sn}/Cr_{Sn}: 0.86 eV.

From the measured chemical diffusion coefficients, characteristic times of drift processes could be estimated. Even though referring to the lower limit of the diffusion coefficients, these estimated times were shorter than actual characteristic times reported in the literature: This suggests that the kinetics of drift processes in Taguchi sensors (at least for the conditions discussed) are controlled by the surface exchange reaction rather than by the chemical diffusion of oxygen.

Acknowledgment

The authors would like to thank Professor Helbig at the University of Erlangen for supplying some of the SnO_2 crystals.

References

[1] W. Göpel, K. Schierbaum, H.-D. Wiemhöfer, J. Maier, Solid State Ionics 32/33 (1989) 440–443.
[2] J. Jamnik, B. Kamp, R. Merkle, J. Maier, Solid State Ionics 150 (2002) 157–166.
[3] J. Maier, W. Göpel, J. Solid State Chem. 72 (1988) 293–302.
[4] W. Hellmich, C. Bosch-v.Braunmühl, G. Müller, G. Sberveglieri, M. Berti, C. Perego, Thin Solid Films 263 (1995) 231–237.
[5] S. Samson, C.G. Fonstadt, J. Appl. Phys. 44 (1973) 1618.
[6] G.N. Advani, P. Klugeweiss, R.L. Longini, A.G. Jordan, Int. J. Electron. 48 (1980) 403–411.
[7] K. Sasaki, J. Maier, Phys. Chem. Chem. Phys. 2 (2000) 3055–3061.
[8] J. Mizusaki, H. Koinuma, J.-I. Shimoyama, M. Kawasaki, K. Fueki, J. Solid State Chem. 88 (1990) 443–450.
[9] L.Z. Yang, Z.T. Sui, C.Z. Wang, Solid State Ionics 50 (1992) 203–208.
[10] T. Sakurai, T. Takizawa, High Temp. High Pressures 3 (1971) 325–331.
[11] Y. Dusausoy, R. Ruck, J.M. Gaite, Phys. Chem. Minerals 15 (1988) 300–303.
[12] J. Maier, J. Am. Ceram. Soc. 76 (1993) 1212–1232.
[13] J. Maier, W. Münch, J. Chem. Soc. Farad. Trans. 92 (1996) 2143–2149.
[14] B. Thiel, R. Helbig, J. Cryst. Growth 32 (1976) 259–264.
[15] B. Kamp, R. Merkle, J. Maier, Sensors Actuators B 77 (2001) 534–542.
[16] A.F. Hollemann, E. Wiberg, Lehrbuch der Anorganischen Chemie, Auflage, Walter de Gruyter Verlag, Berlin, 1985, pp. 91–100.
[17] J.E. Huheey, Anorganische Chemie, De Gruyter, Berlin/New York, 1988.
[18] H.S. Carlslaw, J.C. Jaeger, Conduction of Heat in Solids, Clarendon Press, Oxford (UK), 1959.
[19] T.B. Reed, J.T. Roddy, A.N. Mariano, J. Appl. Phys. 33 (1962) 1014–1015.
[20] B. Kamp, Ph.D. Thesis, University of Stuttgart, 2002.
[21] J. Maier, J. Jamnik, M. Leonhardt, Solid State Ionics 129 (2000) 25–32.
[22] H.J. van Daal, Solid State Commun. 6 (1968) 5–9.
[23] M. Nagasawa, S. Shinoya, S. Makishim, J. Phys. Soc. Japan 20 (1965) 1093.
[24] H. Koch, Phys. Stat. Sol. 3 (1963) 1619–1628.
[25] C.G. Fonstad, R.H. Rediker, J. Appl. Phys. 42 (1971) 2911–2918.
[26] H.I. Yoo, C.E. Lee, J. Am. Ceram. Soc. 88 (2005) 617–623.
[27] G. Blaustein, M.S. Castro, C.M. Aldao, Sensors Actuators B 55 (1999) 33–37.
[28] B. Ruhland, Th. Becker, G. Müller, Sensors Actuators B 50 (1998) 85–94.
[29] V.V. Kissine, S.A. Voroshilov, V.V. Sysoev, Thin Solid Films 348 (1999) 304–311.
[30] S.-C. Chang, J. Vac. Sci. Technol. 17 (1980) 366–369.
[31] V. Lantto, P. Romppainen, Surf. Sci. 192 (1987) 243–264.
[32] G. Sberveglieri, G. Coccoli, P. Benussi, S. Groppelli, P. Nelli, Appl. Surf. Sci. 40 (1989) 169–174.
[33] P.G. Harrison, M.J. Willett, Nature 332 (1988) 337–339.
[34] H. Hikita, K. Takeda, Y. Kimura, Phys. Rev. B 46 (1992) 14381–14386.